ACS APPLIED MATERIALS & INTERFACES

Research Article

www.acsami.org

One-Step Synthesis of Dual Clickable Nanospheres via Ultrasonic-Assisted Click Polymerization for Biological Applications

Yong Hou,[†] Shoupeng Cao,[†] Xueming Li,[†] Beibei Wang,[†] Yuxin Pei,*[,†] Lin Wang,[†] and Zhichao Pei*[,†,‡]

[†]State Key Laboratory of Crop Stress Biology for Arid Areas and College of Science, Northwest A&F University, Yangling, Shaanxi 712100, People's Republic of China

[‡]Attana AB, Stockholm 11419, Sweden

Supporting Information

ABSTRACT: Dual clickable nanospheres (DCNSs) were synthesized in one step using an efficient approach of ultrasonic-assisted azide−alkyne click polymerization, avoiding the need of surfactants. This novel approach presents a direct clickable monomer-to-nanosphere synthesis. Field emission scanning electron microscopy (FESEM), Fourier transform infrared spectroscopy (FTIR), and dynamic laser scattering (DLS) were used to characterize the synthesized DCNSs. Numerous terminal alkynyl and azide groups on the surface of DCNSs facilitate effective conjugation of multiple molecules or ligands onto a single nanocarrier platform under mild conditions. To exemplify the potential of DCNSs in biological applications, (1) multivalent glyconanoparticles (GNPs) were prepared by clicking DCNSs with azide-functionalized and alkyne-functionalized lactose sequentially for the determination of carbohydrate-galectin interactions with quartz crystal microbalance (QCM) biosensor. Using protein chip (purified galectin-3 coated on chip) and cell chip (Jurkat cells immobilized on chip), the QCM sensorgrams showed excellent binding activity of GNPs for galectins; (2) fluorescent GNPs were prepared by clicking DCNSs with azide-functionalized Rhodamine B and alkyne-functionalized lactose sequentially in order to target galectin, which is overexpressed on the surface of Jurkat cells. The fluorescent images obtained clearly showed the cellular internalization of fluorescent GNPs. This fluorescent probe could be easily adapted to drugs to construct lectin-targeted drug delivery systems. Thus, DCNSs prepared with our method may provide a wide range of potential applications in glycobiology and biomedicine.

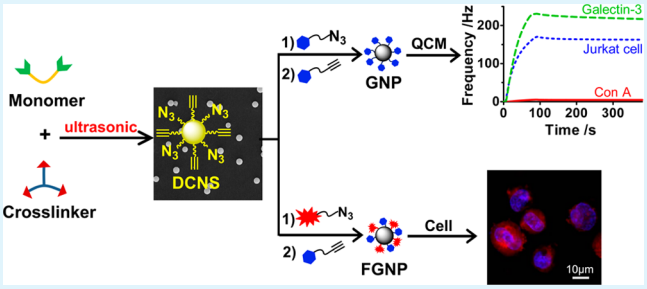

KEYWORDS: *clickable nanospheres, click polymerization, ultrasonic, surfactant-free, carbohydrate-lectin interactions, cell imaging*

INTRODUCTION

Advantages of polymeric nanoparticles (PNPs), including low cytotoxicity,[1,2] biocompatibility,[3] low cost,[4] and functional diversity,[5,6] have led to numerous applications in fabrication of novel materials,[7] nanomedicine,[8] cell imaging,[9] bioanalysis,[10] and other biological areas.[11,12] To enable these applications, various methods have been developed for the production of well-controlled polymer nanoparticles in the past decades. So far, the most successful and commonly used method for the preparation of polymeric nanoparticles is emulsion polymerization, which requires a large amount of surfactants. However, the use of surfactants in emulsion polymerization is costly, environmentally unfriendly, and more importantly, detrimental to the properties of nanoparticles.[13] Surfactants are irremovable from nanoparticle surfaces in many cases.[14] These residues, especially those that are fluorinated, on the surface of nanoparticles are undesirable for many applications including cell imaging and drug delivery. The drawbacks are not only high cytotoxicity[15,16] caused by the surfactants themselves, but also alteration of the biocompatibility and surface properties of nanoparticles, and possible blocking the access to modified surfaces.[17] Therefore, surfactant-free (soap-free) approaches for PNP synthesis are extremely desired. The approaches reported include microwave methodology,[18,19] self-assembly of amphiphilic copolymers,[20,21] copolymerization with surfmers,[22,23] and acoustic emulsification.[13,24] For example, Hawker et al. prepared well-defined nanoparticles (NPs) of poly(methyl methacrylate) (PMMA) with hydroxy functional groups via microwave methodology.[19] By using oligoglycidol macromonomers with linear and branched oligoglycidol structures and variable chain length as surfmers, Pitch et al. prepared copolystyrene NPs.[23] Recently, Atobe et al. developed acoustic emulsification to prepare PMMA NPs. However, the high frequency ultrasonic equipment that is required for this process is hard to obtain, and thus limits its application.[13,24] These approaches usually found their applications in systems with styrene or alkyl acrylates as monomers. It remains a long-standing challenge to develop an approach for PNP synthesis with different monomers to enrich the material diversity of

Received: July 9, 2014
Accepted: September 11, 2014
Published: September 11, 2014

PNPs, which is in urgent demand due to their increasing applications in material chemistry and in biology.

However, bifunctional NPs facilitate the assembly of multiple components in a single nanocarrier platform, which is a pressing need in many biological applications. The work published regarding this includes carboxyl/hydroxyl dual surface-functionalized polystryrene/Fe_3O_4@SiO_2 Janus NPs prepared with miniemulsification[25] and alkynyl/azide surface-functionalized nanogels, via click chemistry between dextrans modified with alkyne or azide groups using conditional inverse emulsion method.[1] Both methods involved the utilization of surfactants. Considering the disadvantages mentioned above, these methods are not favorable, especially from the viewpoint of green process.

Resurrected in 2002,[26] click reaction, known for 1,3-dipolar cycloaddition reaction between azide and alkyne functional groups using Cu(I) as catalyst (CuAAC), has become a powerful polymerization technique in preparation of dendrimers, postfunctionalization of preformed polymers, and generation of functional surfaces.[27−30] Polytriazoles, synthesized via CuAAC, displaying advanced functions, such as aggregation-induced emission,[31,32] thermal stability, biocompatibility,[1,29] and optical nonlinearity,[30] are increasingly gaining attraction.[35] Although there are a few examples of preparing PNPs via click reaction,[1,30] the difficulty lies in avoiding the coalescence of PNPs due to the click reactions occurring between the two existing reactive groups, azide and alkyne. To overcome the coalescence of PNPs in a surfactant-free click polymerization, Tuncel et al.[30] introduced positive charges to the PNPs using diaminodialkyne as a clickable cross-linker; Tang et al.[32] performed click polymerization with unequal number of reactive functional groups of alkyne and azide, so that one type of functional groups can be consumed rapidly to ensure that the polymer is only encapped with the other type of functional groups. However, the trade-off of this method is the synthesis of single-functionalized polymer nanoparticles prepared instead dual ones. To the best of our knowledge, ultrasonic irradiation, a widely used solution for enhancing solubility and particles dispersion,[13] easily accessed from a ultrasonic bath in routine laboratories, has not been used as a measure for resisting the coalescence of PNPs via surfactant-free click polymerizations.

Here, we report a novel synthetic approach for one step synthesis of dual clickable nanospheres (DCNSs), avoiding the need of surfactants, via ultrasonic-assisted alkyne−azide click polymerization catalyzed by $Cu(PPh_3)_3Br$. The monomers and cross-linkers used for click polymerization in this work are listed in Scheme 1. The potential biological applications of DCNSs were exemplified by preparing multivalent glyconanoparticles (GNPs) to detect carbohydrate-galectin interactions with a quartz crystal microbalance (QCM) biosensor and by preparing fluorescent glyconanopaticles (GNPs) for cell imaging, respectively.

RESULTS AND DISCUSSION

To fabricate DCNSs via click polymerization, 3,5- and 2,6-dialkynylpyridine (**1** and **2**) were chosen as the monomers. This is because the rigid structure of 6-member ring can endow polymer nanosphere essential structural rigidity, and the easy formation of quaternary ammonium salt from pyridine[36−38] can be further used to improve hydrophilicity and bactericidal activity[36,39] of DCNSs if required. 1,3-bis(azidoacetoxy)-2-azidoacetoxymethyl-2-ethylpropane (triazide, **3**) and 2,2-bis((2-azidoacetoxy)methyl)propane-1,3-diyl bis(2-azidoacetate) (tetra-azide, **4**) were chosen as the cross-linkers. The alkyne−azide cycloaddition between either of the monomers and either of the cross-linkers, four "monomer + crosslinker" combinations (**1** + **3** or **4** and **2** + **3** or **4**) in total, were catalyzed by $Cu(PPh_3)_3Br$, which is more effective than classical catalysts, such as CuI or CuBr, due to its better solubility in organic solvents.[27] When the click polymerization between monomer **1** and cross-linker **3** was performed with a magnetic stirrer bar, i.e., without ultrasonic-assitance, irregular cauliflower-like particles in micron scale were formed. As expected, heavy adhesion among the particles was observed (Scheme 2a and Supporting Information (SI) Figure S1), as there was no surfactant to stabilize the high surface energy of nanospheres that formed during polymerization.

Ultrasonic irradiation can be used to overcome the nanosphere coalescence arising from their high surface energy[40] via its cavitation effect, which causes high speed impinging liquid jets and strong hydrodynamic shear-force.[41,42] Most importantly, with ultrasonic assistance, nanoparticles can be

Scheme 1. Chemical Structures of Monomers (1,2) and Crosslinkers (3,4) Used for Synthesis of DCNSs

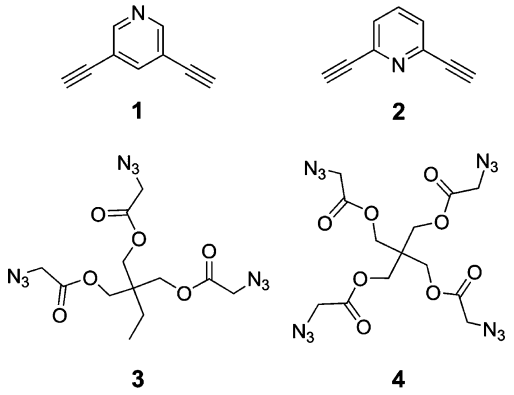

Scheme 2. Synthesis of DCNSs with Monomer 1 and Crosslinker 3 in $CH_3CN/CHCl_3$ (96:4 in Volume)[a]

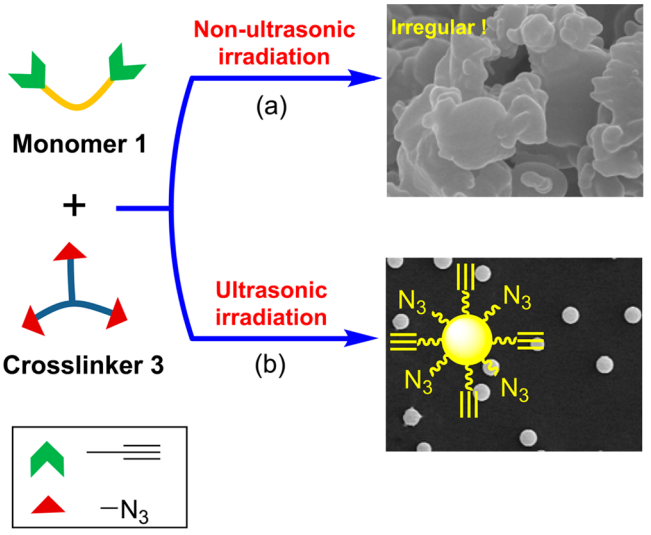

[a](a) stirring at room temperature leading to the formation of irregular polymer particles; (b) ultrasonic irradiation leading to the formation of nanoshperes.

dx.doi.org/10.1021/am504479w | ACS Appl. Mater. Interfaces 2014, 6, 16909−16917

formed in the absence of surfactants, which avoids all the possible problems resulting from the residue of surfactants on the nanoparticles. In this work, to inhibit coalescence among nanospheres in the absence of surfactants, ultrasonic irradiation was applied throughout the polymerization process.

Under ultrasonic irridation of 40 kHz, we explored the polymerization between **1** and **3** (Scheme 2) in a few different polar aprotic solvents because of their crucial role in determining the morphology of nanoparticles.[43] The solvents affected the morphology of the polymer particles via their different collapse speed of cavitation bubbles produced by ultrasonic waves, where different surface tension and viscosity of the solvents resulted in variation in pressure inside the bubbles.[44] As shown in Figure 1, the morphology of the

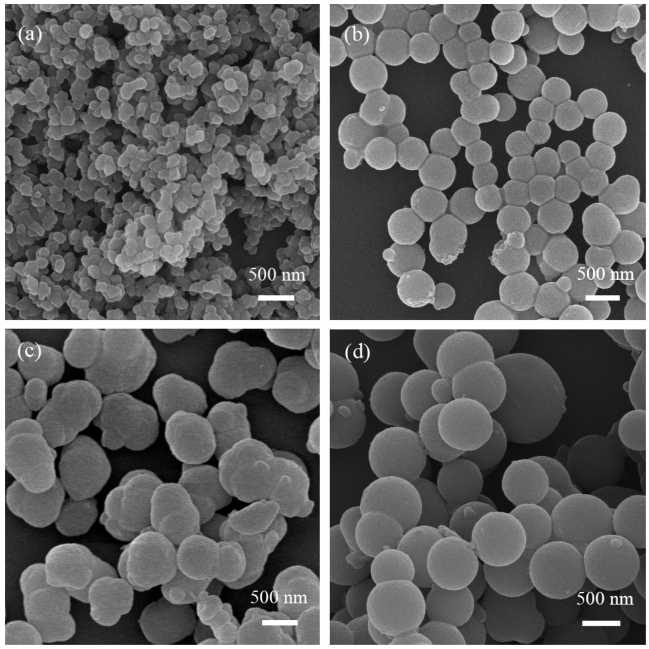

Figure 1. FESEM images of the polymer particles synthesized from **1** + **3** combination under ultrasonic irradiation at 40 kHz: (a) THF; (b) DCM; (c) DMF; and (d) $CH_3CN/CHCl_3$ (96:4 in volume).

particles formed by the polymerization of **1** and **3** varied in different solvents: irregular nanoparticles with heavy adhesion were obtained in tetrahydrofuran (THF) (Figure 1a), slightly adhesive nanospheres with minor distortion were formed in dichloromethane (DCM) (Figure 1b) or DMF (Figure 1c), while nice nanospheres were favored in a solvent mixture of 4 vol % chloroform ($CHCl_3$) in CH_3CN (Figure 1d). Further investigation on the ratio of $CHCl_3$ to CH_3CN disclosed that higher concentration of $CHCl_3$ in the solvent mixture caused structural deformities in the nanospheres as shown in SI Figure S2. Therefore, 4 vol % $CHCl_3$ in CH_3CN was used as the solvent in the following polymerizations.

Our preliminary study showed that ultrasonic irradiation was effective in inhibiting coalescence of nanoparticles in the absence of surfactants. Encouraged by this, we further investigated the effect of frequency on the morphology of polymer particles synthesized from **2** + **3** combination in $CH_3CN/CHCl_3$ (96:4 in volume) with three different frequencies (45, 80, and 100 kHz) for the optimization of dispersion, size, and polydispersity. The results are displayed in Figure 2a–c. Although nice nanospheres were obtained in each

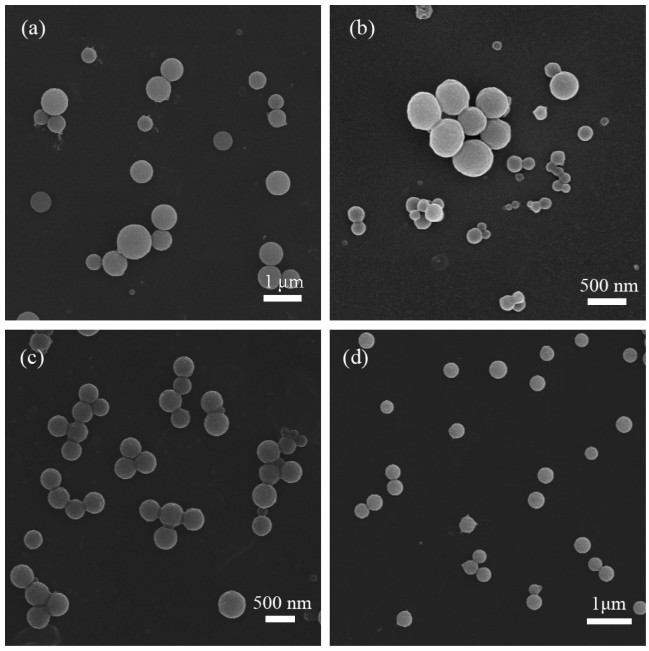

Figure 2. FESEM images of nanospheres synthesized from **2** + **3** combination in $CH_3CN/CHCl_3$ (96:4 in volume). During the polymerization, the reaction mixture was under ultrasonic irradiation of either mono- or multifrequency mode: (a) 45 kHz, (b) 80 kHz, (c) 100 kHz, and (d) multifrequency mode.

case of the three frequencies, one can clearly see that the difference caused by frequency on dispersion, size, and polydispersity of DCNSs: individual DCNSs with a wide size distribution were formed at 45 kHz (Figure 2a); In contrast to 45 kHz, slightly aggregated DCNSs with a narrow size distribution were formed at 100 kHz (Figure 2c). The results above could be explained with the relationship between the radius as well as the range of cavitation bubbles and the frequency. It is known that the possible radius of cavitation bubbles as well as distribution increase inversely to the frequency.[45] The strength of the shear-forces associated with the collapse of cavitation bubbles, responsible for the dispersion of particles, is greater at a lower frequency (45 kHz) than that at a higher one (100 kHz) because of the larger bubbles emerged at lower frequencies. Thus, a lower frequency affords better particle dispersion; however, the distribution of the bubbles, responsible for the homogeneity of monomer concentration and subnano-nuclei, is narrower at a higher frequency. Correspondingly, DCNPs formed at 100 kHz had a narrower distribution.

Surprisingly, at 80 kHz, aggregated DCNSs with two different ranges were obtained (Figure 2b), not showing any advantage either in size distribution (comparing with 45 kHz) or dispersion (comparing with 100 kHz). A tentative explanation could be that the shear-force produced at 80 kHz is not strong enough to prevent the coalescence of nuclei; alternatively, the distribution of microbubbles is not narrow enough to provide homogeneous monomer concentration in the vicinity of the nuclei. Accordingly, coalesced particles with two different distributions formed at 80 kHz.

On the basis of this conjecture, we assumed that a multifrequency mode of ultrasonic irradiation with a prolongation of the time under 45 kHz and 100 kHz should benefit the formation of nanoparticles with relatively narrow

size distribution with good dispersion. Delightfully, the best result was obtained with a multifrequency mode (tandem repeats of 45 s cycles of different frequency during polymerization with fixed time periods: 45 kHz for 15 s, 80 kHz for 5 s, 100 kHz for 25 s), as shown in Figure 2d. Dynamic laser scattering (DLS) analysis indicated the formation of nanospheres under the multifrequency mode with a narrow size distribution centered at a hydrodynamic diameter (D_H) of 282 nm with a polydispersity index (PDI) of 0.413.

With these findings in hand, the optimized conditions (multifrequency mode, $CH_3CN/CHCl_3$ 96:4 in volume) for fabricating nanospheres was further applied to other "monomer + crosslinker" combinations, including **1** + **3**, **1** + **4**, and **2** + **4**. As can be seen in Figure 3, nanospheres from **1** + **3** (Figure 3a), **1** + **4** (Figure 3b), and **2** + **4** (Figure 3c) were successfully synthesized. The results are summarized in Table 1. To the best of our knowledge, this is the first report for a single step monomer-to-nanosphere synthesis, with consideration of dual surface functionalization of NSs and surfactant-free polymerization.

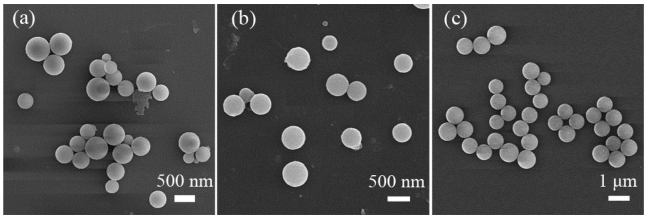

Figure 3. FESEM images of the nanospheres synthesized from **1** + **3** (a), **1** + **4** (b), and **2** + **4** (c) combination in $CH_3CN/CHCl_3$ (96:4 in volume) under multifrequency mode. The polymerization were catalyzed by $Cu(PPh_3)_3Br$ (15 mol %) at 13 °C for 3 h.

Table 1. Summary of DCNSs under the Optimal Conditions[a]

entry	monomer + cross-linker	D_H[b] (nm)	PDI[b]	FESEM
1	1 + 3	553 ± 75	0.453	Figure 3a
2	1 + 4	495 ± 59	0.298	Figure 3b
3	2 + 3	282 ± 36	0.413	Figure 2d
4	2 + 4	766 ± 63	0.287	Figure 3c

[a]Reaction conditions: monomer/cross-linker = 1:1 equiv, $Cu(PPh_3)_3Br$ 15 mol %, 13 °C, 3 h. $CH_3CN/CHCl_3$ (96:4 in volume), multifrequency mode. [b]Average values of three measurements by DLS (SI Figure S3).

The corresponding DCNSs were characterized by DLS (SI Figure S3) and FTIR (SI Figure S4), respectively. DLS analysis showed the nanospheres with D_H between 282 ± 36–766 ± 63 nm and PDI between 0.287 and 0.453 could be obtained with our approach. The terminal alkynyl and azide groups on DCNSs were confirmed by FTIR spectra with the absorption at 3245, 2106, and 2097 cm^{-1} ascribed to C—H, C≡C in propargyl and azide functionality, respectively.[46]

On the basis of the existence of terminal alkynyl and azide groups on NPs synthesized in our work, we predict that, theoretically, any azide- or alkyne-functionalized molecule (so-called "clickable molecule") can be effectively conjugated to DCNSs via click chemistry; Hence, specific products can be formed under mild conditions.

To exemplify the potential of DCNSs in biological applications, first, DCNSs were used to prepare GNPs by clicking with azide- and alkyne-functionalized lactose (**5** and **6** in Scheme 3) sequentially, which were then applied in the detection of carbohydrate-lectin binding affinity with QCM biosensor.

Scheme 3. Chemical Structures of Alkyne- and Azide-Functionalized Compounds

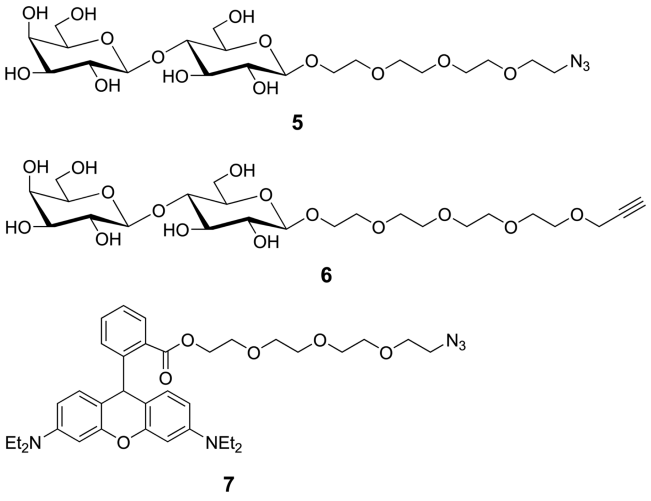

5 **6** **7**

Carbohydrate-lectin recognition plays important roles in fertilization, immune function, and cellular adhesion. However, binding affinity of lectins for individual monosaccharide units is rather weak.[47−49] Hence, multivalent glycoconjugates for generating strong interactions for lectins, so-called Glycoside Cluster Effect, are particularly in need.[50] With DCNSs synthesized using our approach, the simple preparation of GNPs was as following: catalyzed by $CuSO_4$/sodium ascorbate, DCNSs were sequentially conjugated with azide-functionalized lactose (**5**) and alkyne-functionalized lactose (**6**) at room temperature sequentially in two separate steps. GNPs were obtained after dialysis against PBS buffer (Figure 4A upper route). The FESEM image of GNPs showed that the surface of nanospheres became slightly rough (Figure 5a). The FTIR spectra showed that the characteristic absorption peaks of alkynyl group and azide group disappeared; a new broad peak ranging from 3681 to 3021 cm^{-1}, which corresponds to the stretching absorption of hydroxyl groups in lactose, appeared after modification (Figure 5b). Furthermore, the surface of hydrophobic DCNSs turned hydrophilic as they became covered by a layer composed of lactose and hydrophilic chain of PEG. These results indicated that lactose molecules were successfully conjugated to DCNSs. The hydrophilicity of GNPs was adequate to allow a stable aqueous emulsion solution suitable for QCM measurement.

QCM biosensor is a label-free and real-time sensor technology for measuring biomolecular interactions.[51−53] In our experiments, carbohydrate−protein interactions were measured by QCM biosensor with protein chip and cell chip, respectively. Protein chip is a traditional biochip, which is limited to immobilizing isolated and purified target proteins from cells on sensor surfaces. Cell chip is fabricated by growing or capturing cells onto sensor surfaces, where binding events take place, more closely mimicking a native environment.[54] Although the binding data obtained from protein chip do not

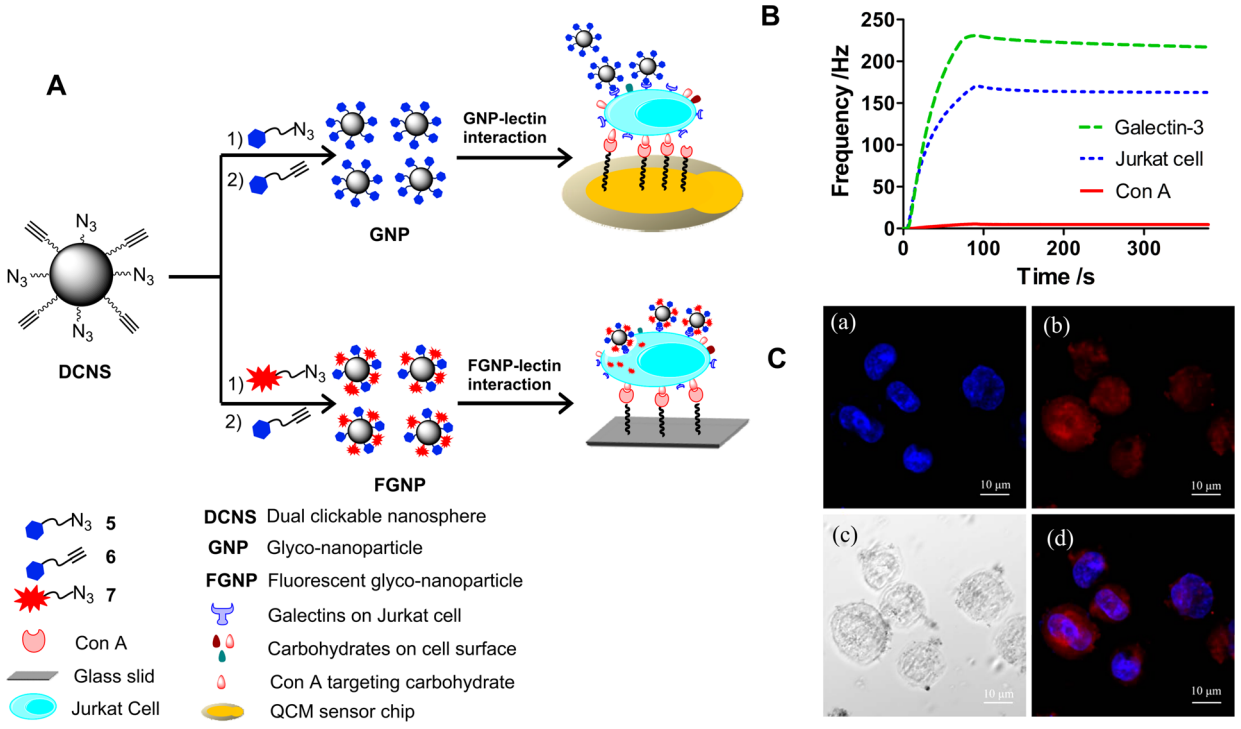

Figure 4. Schematic illustration of the preparation and application of GNPs and FGNPs: **A** Upper route: preparation of GNPs via dual click reactions and application to QCM biosensor; Lower route: preparation of FGNPs via dual click reactions and application to cell imaging. **B** Frequency shifts caused by interaction of GNPs with galectin-3 (dashed line), galectins on surface of Jurkat cells (dotted line), and Con A (solid line, control) immobilized on a QCM biosensor surface, respectively. **C** Confocal fluorescence images of Jurkat cells after incubation with FGNPs (50 μg/mL) for 30 min: (a) nuclei stained with Hoechst 33342 blue; (b) cell membrane (RhB channel); (c) bright field; and (d) merged image of (a) and (b).

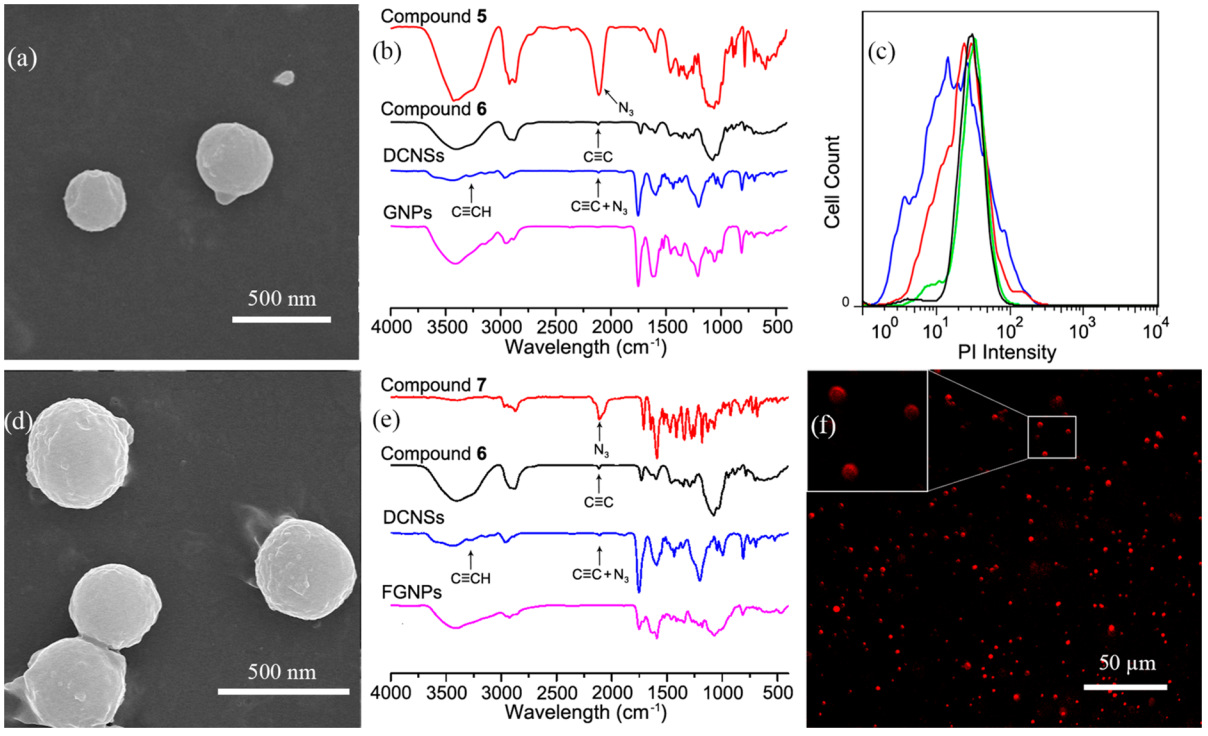

Figure 5. (a) FESEM image of GNPs; (b) IR spectra of GNPs; (c) Viability studies of Jurkat cells. The cells were stained with PI prior to analysis, and viability was assessed immediately after incubation with flow cytometry: control (black), cells treated with GNPs (200 μg/mL) for 12 h (green), 24 h (red), and 48 h (blue); (d) Rhodamine-labeled GNPs (FGNPs) image by FESEM; and (e) IR spectra of FGNPs; (f) LSCM image of FGNPs, the inset on upper-left is an enlarged view of FGNPs for the marked area.

dx.doi.org/10.1021/am504479w | ACS Appl. Mater. Interfaces 2014, 6, 16909−16917

present the biological contexts and do not reflect their native functions in cells accurately, it can be used as a control for comparison with that obtained from cell chip. The emulsion of GNPs (1 mg/mL in PBS buffer) was applied to detect their binding activity with galectins (lactose-specified lectins). The binding value was recorded as the resulting frequency shifts of the quartz crystal. The QCM sensorgrams (Figure 4B) showed excellent binding activity of GNPs for galectins using protein chip (purified galectin-3 coated on chip, specific control) and cell chip (Jurkat cells[55] immobilized on chip) with a frequency shift of 234 and 170 Hz, respectively. Concanavalin A (Con A, does not bind to lactose) was used as a nonspecific control; a frequency shift of only 5 Hz for Con A indicating that the interaction between GNPs and Galectin-3 was specific.

Furthermore, to examine the potential toxicity of GNPs, Jurkat cells were incubated with GNPs (200 μg/mL) for 12, 24, and 48 h, respectively. No obvious apoptosis was observed (Figure 5c), indicating that, as expected, the lactose functionalized nanospheres exhibit excellent biocompatibility.

Fluorescence labeling, despite its many advantages, may affect the bioactivities of directly labeled biomolecules.[56,57] With DCNSs synthesized in this work, we can conveniently combine multivalent fluorescent tags and biomolecules onto a single nanocarrier platform, avoiding any direct labeling on the biomolecules. Following the similar procedure for fabricating GNPs mentioned above, FGNPs could be obtained by replacing one of the two differently tagged lactoses with a clickable fluorescent compound. For example, azide-functionalized Rhodamine B (RhB, **7**), replacement of **5**, was first conjugated to DCNSs, followed by the conjugation of **6** for FGNPs synthesis (Figure 4A lower route). FGNPs were obtained after dialysis against PBS buffer and characterized by FESEM, FTIR, and Laser Scanning Confocal Microscope (LSCM), respectively. The smooth surface of DCNSs became slightly rough, corresponding to the conjugation of lactose and Rhodamine B (Figure 5d); The characteristic absorbance peaks of alkyne and azide disappeared according to the IR spectrum of FGNPs (Figure 5e); FGNPs emitted red fluorescent light under RhB channel with LSCM (Figure 5f). All of these proved the successful conjugation of DCNSs with the clickable ligands. Lactoses on FGNPs acted as targeting ligands for galectins overexpressed on the surface of Jurkat cells,[55] which enabled receptor-mediated endocytosis due to the specific interaction of lactose with galectins.[25,58] The fluorescent images obtained with LSCM (Figure 4C) clearly showed that FGNPs entered the cells after incubating Jurkat cells with FGNPs (50 μg/mL) for 30 min, where FGNPs could be taken up by Jurkat cells through endocytic mechanism during incubation.[59] Moreover, the fluorescent probe could be easily replaced with drugs for constructing lectin-targeted drug delivery system, which is currently underway in our laboratory.

CONCLUSIONS

DCNSs were synthesized for the first time through a one step monomer-to-nanosphere approach of ultrasonic-assisted azide–alkyne click polymerization, avoiding the use of surfactants. DCNSs can be fabricated by choosing suitable solvent system and ultrasonic irradiation mode. The approach developed here may be extended to the synthesis of other types of tailored polymeric NSs. Furthermore, so-fabricated DCNSs are ready for further facile conjugation of clickable ligands, especially sensitive biomolecules, and facilitate incorporation of multiple components onto a single nanocarrier platform under mild conditions, which is a huge advantage for keeping bioactivities of biomolecules. Their biological applications, demonstrated with the detection of carbohydrate-galectin binding interactions via QCM biosensor and fluorescent cell imaging, may expand in diverse research areas, particularly glycobiology and biomedicine.

EXPERIMENTAL SECTION

Materials and Instruments. All chemicals used in this work from commercial sources were used as received. Acetonitrile was dried by CaH_2 and chloroform was distilled before use. The other solvents were used as received. Column chromatography was performed using silica gel with a grain size of 40–63 μm (Qingdao Haiyang Co., Ltd.). 2,6-Dibromopyridine and 3,5-dibromopyridine were purchased from Beijing Datianfengtuo Chemistry Co., Ltd. Tetraglycol, trimethylol propane, and pentaerythritol were obtained from Aladdin. 1-Ethyl-3-[3-dimethylaminopropyl] carbodiimide hydrochloride (EDC), *N*-hydroxysulfosuccinimide (sulfo-NHS), ethanolamine (1 M, pH 8.5), Concanavalin A (Con A), and the blue nucleic acid stain Hoechst 33342 were purchased from Sigma. Galectin-3 was obtained from Sino Biological Inc. Jurkat cells were kindly provided by Prof. Bin Gao at Institute of Microbiology, Chinese Academy of Sciences (IMCAS).

^{1}H and ^{13}C NMR spectra were recorded on a Bruker Advance 500 instrument in $CDCl_3$, using the residual signals from $CHCl_3$ (^{1}H: δ 7.26 ppm; ^{13}C: δ 77.0 ppm) as internal standard. HRMS (High Resolution Mass Spectrometer) analysis was performed on an Agilent 1290–6540 UHPLC Q-Tof-HRMS. Infrared spectra were measured using KBr pellets and recorded on an FTIR-instrument (BRUKER TENSOR 27, Germany). The Dynamic Light Scattering (DLS) data was obtained by Delsa Nano C analyzer (Beckman Coulter, Inc.). Field emission scanning electron microscopy (FESEM) images were taken on a Hitachi-S4800 instrument operated at 10 kV. A Laser Scanning Confocal Microscope (LSCM, Carl Zeiss LSM 510 UVMETA, Germany) was used to capture images of the cells after incubation with fluorescent glyconanoparticles. Ultrasonic irradiation was produced by SB-5200DT monofrequency ultrasonic cleaner (Ningbo Scientz Biotechnology Co., Ltd.) or KQ-300VDB multifrequency ultrasonic cleaner (Kun Shan Ultrasonic Instruments Co., Ltd.). The centrifuge was performed with H1650–W table-top micro capacity high-speed centrifuge (Hu Nan Xiang Yi Instruments Co., Ltd.). Biosensor experiments were undertaken using an Attana Cell A200 QCM instrument (Attana AB, Stockholm, Sweden) at 22 °C and the running buffer was phosphate buffered saline (PBS) at pH 7.2.

Synthesis of Compound 1–7. Synthesis of compounds **8–11** can be found in the SI.

*3,5-Diethynylpyridine (**1**).*[60] To a 250 mL flask, Compound **8** (2.0 g, 8.23 mmol) and KOH (0.92 g, 16.5 mmol) were added into 100 mL of Ar-degassed toluene, the resulting solution was refluxed for 12 h. The solvent was removed under vacuum to leave a yellow brown solid, which was then dissolved in dichloromethane. The solution was filtered and the filtrate was dried under vacuum to give a yellow brown solid. Purification by column chromatography on silica gel afforded a white powder of **1** (0.53 g, 51%). ^{1}H NMR (400 MHz, $CDCl_3$) δ 8.65 (d, J = 1.9 Hz, 2H), 7.88 (t, J = 1.9 Hz, 1H), 3.26 (s, 2H) ppm. ^{13}C NMR (126 MHz, $CDCl_3$) δ 151.95, 141.90, 119.00, 81.44, 79.39 ppm.

*2,6-Diethynylpyridine (**2**).*[61] To a 50 mL flask, Compound **9** (1.02 g, 3.76 mmol) was dissolved in 20 mL of MeOH, followed by addition of K_2CO_3 (2.59g, 18.8 mmol). The mixture was stirred for 12 h at room temperature. The solvent was evaporated under vacuum. 50 mL CH_2Cl_2 was added to the residue, and the insoluble solids were filtered away. The filtrate was washed with saturated brine (2 × 30 mL), and the organic phase was dried over Na_2SO_4. After removing the solvent, the crude was purified by flash chromatography on silica gel to afford a white solid (0.38 g, 79%). ^{1}H NMR (400 MHz, $CDCl_3$) δ 7.67 (t, J = 2 Hz, 1H), 7.46 (d, J = 2 Hz, 2H), 3.18 (s, 2H) ppm. ^{13}C NMR (126 MHz, $CDCl_3$) δ 142.75, 136.56, 127.12, 82.11, 76.81 ppm.

*1,3-Bis(azidoacetoxy)-2-azidoacetoxymethyl-2-ethylpropane (**3**).*[62] To a 25 mL flask, 1,3-Bis(chloroacetoxy)-2-chloroacetoxymethyl-2-ethylpropane (3.63 g, 10 mmol) was dissolved in 30 mL DMSO,

NaN_3 (2.93 g, 45 mmol) was added with cooling. The reaction mixture was slowly warmed to 40 °C and stirred for 2 days. The reaction mixture was then poured into ice water and extracted with dichloromethane (3 × 30 mL). The dichloromethane extract was washed 3 times with brine and then dried over Na_2SO_4. Evaporation of the solvent and purification by column chromatography on silica gel afforded **3** as a colorless liquid (2.41 g, 63%). ^{1}H NMR (500 MHz, $CDCl_3$) δ 4.19 (s, 6H), 3.91 (s, 6H), 1.54 (q, J = 7.6 Hz, 2H), 0.94 (t, J = 7.6 Hz, 3H) ppm. ^{13}C NMR (126 MHz, $CDCl_3$) δ 168.02, 64.67, 50.35, 41.12, 22.98, 7.27 ppm.

2,2-Bis((2-azidoacetoxy)methyl)propane-1,3-diyl bis(2-azidoacetate) (4).[62] To a 25 mL flask, 2,2-bis((2-chloroacetoxy)methyl)-propane-1,3-diyl bis(2-chloroacetate) (4.42 g, 10 mmol) was dissolved in 30 mL DMSO, NaN_3 (3.9 g, 60 mmol) was added with cooling. The reaction mixture was slowly warmed to 50 °C and stirred for 2 days. The reaction mixture was then poured into ice water and extracted with dichloromethane (3 × 30 mL). The dichloromethane extract was washed 3 times with brine and then dried over Na_2SO_4. Evaporation of the solvent and purification by column chromatography on silica gel afforded **4** as a colorless oil (2.53 g, 54%). ^{1}H NMR (400 MHz, $CDCl_3$) δ 4.30 (s, 8H), 3.94 (s, 8H) ppm. ^{13}C NMR (125 MHz, $CDCl_3$) δ 167.84, 62.80, 50.29, 42.58 ppm.

2-(2-{2-[2-(2-Azido-ethoxy)-ethoxy]-ethoxy}-ethyl) β-D-galactopyranosyl-(1 →4)-β-D-glucopyranoside (5).[63] To a solution of Compound **10** (840 mg, 1 mmol) in dry MeOH (10 mL), CH_3ONa (54 mg, 1 mmol) was added. The reaction mixture was stirred at room temperature for 2 h. The solution was then neutralized by addition of ion-exchange resin (Amberlite IR 120 H^+) until pH = 7, filtered, and the solvent was removed under reduced pressure for the final product as a white solid (567 mg, 97%). ^{1}H NMR (500 MHz, D_2O) δ 4.42 (d, J = 7.9 Hz, 1H), 4.36 (d, J = 7.8 Hz, 1H), 3.98 (dt, J = 8.2, 3.9 Hz, 1H), 3.89 (d, J = 11.7 Hz, 1H), 3.83 (d, J = 2.9 Hz, 1H), 3.79−3.48 (m, 21H), 3.46 (d, J = 8.1 Hz, 1H), 3.42 (t, J = 4.9 Hz, 2H), 3.26 (t, J = 8.2 Hz, 1H) ppm. ^{13}C NMR (126 MHz, D_2O) δ 102.98, 102.14, 78.43, 75.36, 74.78, 74.33, 72.84, 72.57, 70.97, 69.70, 69.61, 69.59, 69.58, 69.55, 69.23, 68.71, 68.57, 61.02, 60.10, 50.16 ppm.

3,6,9,12-Tetraoxapentadec-14-ynyl (β-D-galactopyranosyl)-(1→4)-β-D-glucopyranoside (6).[64] To a solution of Compound **11** (850 mg, 1 mmol) in dry MeOH (10 mL), CH_3ONa (54 mg, 1 mmol) was added. The reaction mixture was stirred at room temperature for 2 h. The reaction mixture was neutralized by addition of Amberlite IR120 H^+ until pH = 6. The resin was filtered off and the filtrate was dried under vacuum to give the product as a white solid (550 mg, 99%). ^{1}H NMR (500 MHz, D_2O) δ 4.54 (d, J = 8.0 Hz, 1H), 4.47 (d, J = 7.8 Hz, 1H), 4.27 (d, J = 2.1 Hz, 2H), 4.05−4.14 (m, 1H), 4.00 (d, J = 10.8 Hz, 1H), 3.95 (d, J = 3.1 Hz, 1H), 3.89−3.53 (m, 24H), 3.37 (t, J = 8.5 Hz, 1H), 2.92 (s, 1H) ppm. ^{13}C NMR (126 MHz, D_2O) δ 102.97, 102.13, 79.39, 78.43, 76.03, 75.37, 74.79, 74.32, 72.83, 72.56, 70.97, 69.70, 69.61, 69.57, 69.44, 68.76, 68.68, 68.57, 61.03, 60.12, 57.92 ppm.

Azide-Functionalized Rhodamine B (7). To a 25 mL round-bottom flask with a stirrer bar, Rhodamine B (409 mg, 0.85 mmol) and 2-(2-(2-(2-azidoethoxy)ethoxy)ethoxy)ethan-1-ol (100 mg, 0.57 mmol) were dissolved in 10 mL CH_2Cl_2, followed by EDC (326 mg, 1.17 mmol) and 4-(dimethylamino)pyridine (DMAP, 5 mg, 0.04 mmol). The reaction mixture was stirred at room temperature overnight. The solvent was removed under reduced pressure. Purification by flash chromatography on silica gel (CH_2Cl_2/CH_3OH 30:1 to 10:1 in volume) afforded compound **7** (389.5 mg, 0.60 mmol, 71%) as a thick red oil. R_f = 0.35 (CH_2Cl_2/CH_3OH, 10:1 in volume). ^{1}H NMR (500 MHz, $CDCl_3$) δ 8.34−8.28 (m, 1H, Ar—H), 7.80 (t, J = 7.5 Hz, 1H, Ar—H), 7.72 (t, J = 7.8 Hz, 1H, Ar—H), 7.28 (d, J = 7.5 Hz, 1H, Ar—H), 7.08−7.02 (m, 2H, Ar—H), 6.89 (dd, J = 9.5, 2.4 Hz, 2H, Ar—H), 6.79 (t, J = 5.7 Hz, 2H, Ar—H), 4.16 (t, J = 4.6 Hz, 2H, —$COOCH_2$—), 3.68−3.51 (m, 21H, —OCH_2CH_2O—, Ar—CH), 3.36−3.32 (m, 2H, N_3—CH_2—), 1.28 (t, J = 7.1 Hz, 12H, —CH_3) ppm. ^{13}C NMR (126 MHz, $CDCl_3$) δ 165.06, 159.03, 157.92, 155.69, 133.83, 133.33, 131.67, 131.49, 130.53, 130.35, 129.86, 114.39, 113.71, 96.43, 70.78, 70.72, 70.62, 70.16, 68.83, 64.83, 50.82, 46.30, 12.82 ppm. ESI HRMS: Calcd for $C_{36}H_{47}N_5O_6$ $[M - H]^-$: 644.3448, found 644.3454. The ^{1}H NMR, ^{13}C NMR, COSY, and HRMS data of compound **7** were showed in SI Figures S5−S8.

Synthesis of DCNSs. A typical procedure for fabrication of polymeric nanospheres was as following: To a 10 mL flask, monomer (75 μmol), cross-linker (1 equiv), and 2.4 mL dry CH_3CN were added. The flask was put into an ultrasonic water bath and a certain amount of $Cu(PPh_3)_3Br$ in 100 μL dry chloroform was injected. The mixture was exposed to ultrasonic irradiation in a specified mode at 13 °C for a specified time. The final emulsion was centrifuged at 16500 rpm and the precipitate was washed 3 times with chloroform and dried in vacuum. The yield of DCNSs is around 6−10% (the yield of diyne and triazide type is about 6−7%, and nearly 9−10% for diyne and tetra-azide type). The synthesized DCNSs were characterized by DLS, FESEM, and FTIR.

Preparation of Lactose-Modified Nanoparticles (GNPs). The GNPs were prepared according to the following: (1) To a suspension of DCNSs (10.0 mg) in CH_3OH/H_2O (6 mL, 5:1 in volume), azide-functionalized lactose (**5**, 10.0 mg), $CuSO_4{\cdot}5H_2O$ (7.5 mg) and sodium ascorbate (12 mg) were added. The mixture was stirred at room temperature for 24 h. The yellow emulsion was centrifuged at 16 500 rpm. The precipitate was washed three times with H_2O and one time with methanol. (2) Use alkyne-functionalized lactose (**6**, 10 mg) to replace **5**, repeat the process with the precipitate obtained in Step (1). Finally, the reaction mixture was dialyzed using a dialysis membrane (8000−14 000 MWCO) against PBS buffer to remove residual small molecules to obtain GNPs buffer emulsion. GNPs were characterized by FESEM and FTIR (Figure 5a,b).

Preparation of Rhodamine-Labeled Glyconanoparicles (FGNPs). FGNPs were prepared in two steps: (1) To a suspension of DCNSs (10.0 mg) in chloroform (6 mL), azide-functionalized Rhodamine B (**7**, 10.0 mg) and $Cu(PPh_3)_3Br$ (6.8 mg) were added. The mixture was stirred at rt for 24 h. The dark red emulsion was centrifuged at 16 500 rpm. The precipitate was washed 3 times with chloroform. (2) The precipitate obtained in Step (1) was dispersed in CH_3OH/H_2O (6 mL, 5:1 in volume). Following the process described in GNPs preparation, alkyne-functionalized lactose (**6**, 10 mg) was conjugated to the surface of the nanospheres. The final emulsion was dialyzed using a dialysis membrane (8000−14 000 MWCO) against PBS buffer to remove residual small molecules. FGNPs were characterized by FESEM, LSCM, and FTIR (Figure 5d−f).

Interaction between GNPs and Galectin-3, Jurkat Cells or Con A by QCM. The protein (galectin-3 or Con A) and Jurkat cell chips were fabricated by following the published procedures.[65] For measuring the carbohydrate-lectin interaction, each of the sensor chips was inserted into the instrument and allowed to stabilize (baseline drift <0.2 Hz/min) under a continuous flow (20 μL/min) of running buffer (PBS buffer, pH = 7.2). GNPs emulsion in PBS buffer (1 mg/mL) was injected over the surface of the chips, allowed to bind for 105 s, and dissociate for 295 s. The frequency shifts associated with binding events were recorded with the Attester software (Attana, Sweden) in real time.

Sample for Cell Imaging by LSCM. Jurkat cells, cultured according to the standard method,[65] were immobilized on the surface of carboxyl-modified coverslip (20 × 20 mm^2) by following the procedure published previously.[66] In brief, 8 × 10^7 Jurkat cells were seeded onto the Con A-coated coverslip with 1.8 mL PBS in a 6-well plate (Thermo) and incubated at room temperature for 0.5 h. After the cells were immobilized on the modified glass surface, 200 μL FGNPs emulsion was added. The final FGNPs concentration was 50 μg/mL. The plate was incubated at room temperature for 30 min to allow FGNPs interacte with galectins on the cell surface. The cells were rinsed 3 times with PBS, fixed with 3.7% formaldehyde for 10 min. The nuclei of the cells were stained with Hoechst 33 342 and the cells were rinsed with PBS buffer. The cells were then imaged by LSCM.

■ ASSOCIATED CONTENT

Supporting Information

The synthesis of Compound **8**−**11**, additional FESEM images, DLS data, HRMS, NMR, and FTIR spectra. This material is available free of charge via the Internet at http://pubs.acs.org/.

■ AUTHOR INFORMATION

Corresponding Authors

*E-mail: peiyx@nwafu.edu.cn.
*E-mail: peizc@nwafu.edu.cn.

Notes

The authors declare no competing financial interest.

■ ACKNOWLEDGMENTS

We thank the National Natural Science Foundation of China for financial support (NSFC21174113 and 31270861). The authors thank Mr. Yihan Pei (Clare College, Cambridge) for help with the language.

■ REFERENCES

(1) Heller, D. A.; Levi, Y.; Pelet, J. M.; Doloff, J. C.; Wallas, J.; Pratt, G. W.; Jiang, S.; Sahay, G.; Schroeder, A.; Schroeder, J. E.; Chyan, Y.; Zurenko, C.; Querbes, W.; Manzano, M.; Kohane, D. S.; Langer, R.; Anderson, D. G. Modular "Click-in-Emulsion" Bone-Targeted Nanogels. *Adv. Mater.* **2013**, *25*, 1449−1454.

(2) Zhang, X.; Zhang, X.; Yang, B.; Hui, J.; Liu, M.; Chi, Z.; Liu, S.; Xu, J.; Wei, Y. Novel Biocompatible Cross-Linked Fluorescent Polymeric Nanoparticles Based on an AIE Monomer. *J. Mater. Chem. C* **2014**, *2*, 816−820.

(3) Wu, H.; Yang, R.; Song, B.; Han, Q.; Li, J.; Zhang, Y.; Fang, Y.; Tenne, R.; Wang, C. Biocompatible Inorganic Fullerene-Like Molybdenum Disulfide Nanoparticles Produced by Pulsed Laser Ablation in Water. *ACS Nano* **2011**, *5*, 1276−1281.

(4) Poma, A.; Guerreiro, A.; Whitcombe, M. J.; Piletska, E. V.; Turner, A. P. F.; Piletsky, S. A. Solid-Phase Synthesis of Molecularly Imprinted Polymer Nanoparticles with a Reusable Template- "Plastic Antibodies". *Adv. Funct. Mater.* **2013**, *23*, 2821−2827.

(5) Zhang, S.; Zou, J.; Zhang, F.; Elsabahy, M.; Felder, S. E.; Zhu, J.; Pochan, D. J.; Wooley, K. L. Rapid and Versatile Construction of Diverse and Functional Nanostructures Derived from a Polyphosphoester-Based Biomimetic Block Copolymer System. *J. Am. Chem. Soc.* **2012**, *134*, 18467−18474.

(6) Shen, Y.; Zhao, L.; Qi, L.; Qiao, J.; Mao, L.; Chen, Y. Reactive Polymer as a Versatile Toolbox for Construction of Multifunctional Superparamagnetic Nanocomposites. *Chem.—Eur. J.* **2012**, *18*, 13755−13761.

(7) Bae, J.; Lawrence, J.; Miesch, C.; Ribbe, A.; Li, W.; Emrick, T.; Zhu, J.; Hayward, R. C. Multifunctional Nanoparticle-Loaded Spherical and Wormlike Micelles Formed by Interfacial Instabilities. *Adv. Mater.* **2012**, *24*, 2735−2741.

(8) Sahoo, B.; Devi, K. S.; Banerjee, R.; Maiti, T. K.; Pramanik, P.; Dhara, D. Thermal and pH Responsive Polymer-Tethered Multifunctional Magnetic Nanoparticles for Targeted Delivery of Anticancer Drug. *ACS Appl. Mater. Interfaces* **2013**, *5*, 3884−3893.

(9) Zhang, X.; Zhang, X.; Yang, B.; Hui, J.; Liu, M.; Chi, Z.; Liu, S.; Xu, J.; Wei, Y. A Novel Method for Preparing AIE Dye Based Cross-Linked Fluorescent Polymeric Nanoparticles for Cell Imaging. *Polym. Chem.* **2014**, *5*, 683−688.

(10) El-Boubbou, K.; Gruden, C.; Huang, X. Magnetic Glyco-Nanoparticles: A Unique Tool for Rapid Pathogen Detection, Decontamination, and Strain Differentiation. *J. Am. Chem. Soc.* **2007**, *129*, 13392−13393.

(11) Zhao, Z.; Meng, H.; Wang, N.; Donovan, M. J.; Fu, T.; You, M.; Chen, Z.; Zhang, X.; Tan, W. A Controlled-Release Nanocarrier with Extracellular pH Value Driven Tumor Targeting and Translocation for Drug Delivery. *Angew. Chem., Int. Ed.* **2013**, *52*, 7487−7491.

(12) Bao, B.; Ma, M.; Chen, J.; Yuwen, L.; Weng, L.; Fan, Q.; Huang, W.; Wang, L. Facile Preparation of Multicolor Polymer Nanoparticle Bioconjugates with Specific Biorecognition. *ACS Appl. Mater. Interfaces* **2014**, *6*, 11129−11135.

(13) Nakabayashi, K.; Kojima, M.; Inagi, S.; Hirai, Y.; Atobe, M. Size-Controlled Synthesis of Polymer Nanoparticles with Tandem Acoustic Emulsification Followed by Soap-Free Emulsion Polymerization. *ACS Macro Lett.* **2013**, *2*, 482−484.

(14) Nehilla, B. J.; Allen, P. G.; Desai, T. A. Surfactant-Free, Drug-Quantum-Dot Coloaded Poly(lactide-*co*-glycolide) Nanoparticles: Towards Multifunctional Nanoparticles. *ACS Nano* **2008**, *2*, 538−544.

(15) Zhang, X.; Servos, M. R.; Liu, J. Instantaneous and Quantitative Functionalization of Gold Nanoparticles with Thiolated DNA Using a pH-Assisted and Surfactant-Free Route. *J. Am. Chem. Soc.* **2012**, *134*, 7266−7269.

(16) Lin, Y.-S.; Haynes, C. L. Impacts of Mesoporous Silica Nanoparticle Size, Pore Ordering, and Pore Integrity on Hemolytic Activity. *J. Am. Chem. Soc.* **2010**, *132*, 4834−4842.

(17) Chen, H.; Wang, D.; Yu, Y.; Newton, K. A.; Muller, D. A.; Abruna, H.; DiSalvo, F. J. A Surfactant-Free Strategy for Synthesizing, and Processing Intermetallic Platinum-Based Nanoparticle Catalysts. *J. Am. Chem. Soc.* **2012**, *134*, 18453−18459.

(18) Zhang, W. M.; Gao, J.; Wu, C. Microwave Preparation of Narrowly Distributed Surfactant-Free Stable Polystyrene Nanospheres. *Macromolecules* **1997**, *30*, 6388−6390.

(19) An, Z.; Tang, W.; Hawker, C. J.; Stucky, G. D. One-Step Microwave Preparation of Well-Defined and Functionalized Polymeric Nanoparticles. *J. Am. Chem. Soc.* **2006**, *128*, 15054−15055.

(20) Kryuchkov, V. A.; Daigle, J. C.; Skupov, K. M.; Claverie, J. P.; Winnik, F. M. Amphiphilic Polyethylenes Leading to Surfactant-Free Thermoresponsive Nanoparticles. *J. Am. Chem. Soc.* **2010**, *132*, 15573−15579.

(21) Hickey, R. J.; Haynes, A. S.; Kikkawa, J. M.; Park, S. J. Controlling the Self-Assembly Structure of Magnetic Nanoparticles and Amphiphilic Block-Copolymers: From Micelles to Vesicles. *J. Am. Chem. Soc.* **2011**, *133*, 1517−1525.

(22) Fischer, V.; Landfester, K.; Muñoz-Espí, R. Molecularly Controlled Coagulation of Carboxyl-Functionalized Nanoparticles Prepared by Surfactant-Free Miniemulsion Polymerization. *ACS Macro Lett.* **2012**, *1*, 1371−1374.

(23) Pargen, S.; Willems, C.; Keul, H.; Pich, A.; Möller, M. Surfactant-Free Synthesis of Polystyrene Nanoparticles Using Oligoglycidol Macromonomers. *Macromolecules* **2012**, *45*, 1230−1240.

(24) Nakabayashi, K.; Amemiya, F.; Fuchigami, T.; Machida, K.; Takeda, S.; Tamamitsu, K.; Atobe, M. Highly Clear and Transparent Nanoemulsion Preparation under Surfactant-Free Conditions Using Tandem Acoustic Emulsification. *Chem. Commun.* **2011**, *47*, 5765−5767.

(25) Wang, F.; Pauletti, G. M.; Wang, J.; Zhang, J.; Ewing, R. C.; Wang, Y.; Shi, D. Dual Surface-Functionalized Janus Nanocomposites of Polystyrene/Fe_3O_4@SiO_2 for Simultaneous Tumor Cell Targeting and Stimulus-Induced Drug Release. *Adv. Mater.* **2013**, *25*, 3485−3489.

(26) Kolb, H. C.; Finn, M. G.; Sharpless, K. B. Click Chemistry: Diverse Chemical Function from a Few Good Reactions. *Angew. Chem., Int. Ed.* **2001**, *40*, 2004−2021.

(27) Qin, A.; Lam, J. W.; Tang, B. Z. Click Polymerization: Progresses, Challenges, and Opportunities. *Macromolecules* **2010**, *43*, 8693−8702.

(28) Wu, J.; Gao, C. Sliding Supramolecular Polymer Brushes with Tunable Amphiphilicity: One-Step Parallel Click Synthesis and Self-Assembly. *Macromolecules* **2010**, *43*, 7139−7146.

(29) Han, J.; Li, S.; Tang, A.; Gao, C. Water-Soluble and Clickable Segmented Hyperbranched Polymers for Multifunctionalization and Novel Architecture Construction. *Macromolecules* **2012**, *45*, 4966−4977.

(30) İbrahimova, V.; Ekiz, S.; Gezici, Ö.; Tuncel, D. Facile Synthesis of Cross-Linked Patchy Fluorescent Conjugated Polymer Nanoparticles by Click Reactions. *Polym. Chem.* **2011**, *2*, 2818−2824.

(31) Wang, J.; Mei, J.; Yuan, W.; Lu, P.; Qin, A.; Sun, J.; Ma, Y.; Tang, B. Z. Hyperbranched Polytriazoles with High Molecular Compressibility: Aggregation-Induced Emission and Superamplified Explosive Detection. *J. Mater. Chem.* **2011**, *21*, 4056−4059.
(32) Wang, J.; Mei, J.; Zhao, E.; Song, Z.; Qin, A.; Sun, J. Z.; Tang, B. Z. Ethynyl-Capped Hyperbranched Conjugated Polytriazole: Click Polymerization, Clickable Modification, and Aggregation-Enhanced Emission. *Macromolecules* **2012**, *45*, 7692−7703.
(33) Krovi, S. A.; Smith, D.; Nguyen, S. T. "Clickable" Polymer Nanoparticles: a Modular Scaffold for Surface Functionalization. *Chem. Commun.* **2010**, *46*, 5277−5279.
(34) Wu, W.; Ye, C.; Yu, G.; Liu, Y.; Qin, J.; Li, Z. New Hyperbranched Polytriazoles Containing Isolation Chromophore Moieties Derived from AB_4 Monomers through Click Chemistry under Copper(I) Catalysis: Improved Optical Transparency and Enhanced NLO Effects. *Chem.—Eur. J.* **2012**, *18*, 4426−4434.
(35) Juricek, M.; Kouwer, P. H.; Rowan, A. E. Triazole: A Unique Building Block for the Construction of Functional Materials. *Chem. Commun.* **2011**, *47*, 8740−8749.
(36) Zhao, T.; Sun, G. Hydrophobicity and Antimicrobial Activities of Quaternary Pyridinium Salts. *J. Appl. Microbiol.* **2008**, *104*, 824−830.
(37) Ng, V. W. L.; Tan, J. P. K.; Leong, J.; Voo, Z. X.; Hedrick, J. L.; Yang, Y. Y. Antimicrobial Polycarbonates: Investigating the Impact of Nitrogen-Containing Heterocycles as Quaternizing Agents. *Macromolecules* **2014**, *47*, 1285−1291.
(38) Han, J.; Zheng, Y.; Zheng, S.; Li, S.; Hu, T.; Tang, A.; Gao, C. Water soluble Octa-Functionalized POSS: All-Click Chemistry Synthesis and Efficient Host-Guest Encapsulation. *Chem. Commun.* **2014**, *50*, 8712−8714.
(39) Lalloz, L.; Damas, C.; Brembilla, A.; Clement, R.; Lochon, P. Copolymerization Study of 4-Vinylpyridine with *N*-Dodecylacrylamide. *Eur. Polym. J.* **1997**, *33*, 1099−1103.
(40) Luo, P.; Nieh, T. G.; Schwartz, A. J.; Lenk, T. J. Surface Characterization of Nanostructured Metal and Ceramic Particles. *Mater. Sci. Eng., A* **1995**, *204*, 59−64.
(41) Peshkovsky, A. S.; Peshkovsky, S. L.; Bystryak, S. Scalable High-Power Ultrasonic Technology for the Production of Translucent Nanoemulsions. *Chem. Eng. Proc.: Proc. Intens.* **2013**, *69*, 77−82.
(42) Peshkovsky, S. L.; Peshkovsky, A. S. Matching a Transducer to Water at Cavitation: Acoustic Horn Design Principles. *Ultrason. Sonochem.* **2007**, *14*, 314−322.
(43) Kedia, A.; Kumar, P. S. Solvent-Adaptable Poly-(vinylpyrrolidone) Binding Induced Anisotropic Shape Control of Gold Nanostructures. *J. Phys. Chem. C* **2012**, *116*, 23721−23728.
(44) Okitsu, K.; Ashokkumar, M.; Grieser, F. Sonochemical Synthesis of Gold Nanoparticles: Effects of Ultrasound Frequency. *J. Phys. Chem. B* **2005**, *109*, 20673−20675.
(45) Merouani, S.; Hamdaoui, O.; Rezgui, Y.; Guemini, M. Effects of Ultrasound Frequency and Acoustic Amplitude on the Size of Sonochemically Active Bubbles—Theoretical Study. *Ultrason. Sonochem.* **2013**, *20*, 815−819.
(46) Qin, A.; Lam, J. W. Y.; Jim, C. K. W.; Zhang, L.; Yan, J.; Häussler, M.; Liu, J.; Dong, Y.; Liang, D.; Chen, E.; Jia, G.; Tang, B. Z. Hyperbranched Polytriazoles: Click Polymerization, Regioisomeric Structure, Light Emission, and Fluorescent Patterning. *Macromolecules* **2008**, *41*, 3808−3822.
(47) Munoz, E. M.; Correa, J.; Riguera, R.; Fernandez-Megia, E. Real-Time Evaluation of Binding Mechanisms in Multivalent Interactions: A Surface Plasmon Resonance Kinetic Approach. *J. Am. Chem. Soc.* **2013**, *135*, 5966−5969.
(48) Fasting, C.; Schalley, C. A.; Weber, M.; Seitz, O.; Hecht, S.; Koksch, B.; Dernedde, J.; Graf, C.; Knapp, E. W.; Haag, R. Multivalency as a Chemical Organization and Action Principle. *Angew. Chem., Int. Ed.* **2012**, *51*, 10472−10498.
(49) Seto, H.; Ogata, Y.; Murakami, T.; Hoshino, Y.; Miura, Y. Selective Protein Separation Using Siliceous Materials with a Trimethoxysilane-Containing Glycopolymer. *ACS Appl. Mater. Interfaces* **2012**, *4*, 411−417.
(50) Lee, Y. C.; Lee, R. T. Carbohydrate-Protein Interactions: Basis of Glycobiology. *Acc. Chem. Res.* **1995**, *28*, 321−327.
(51) Pei, Z.; Anderson, H.; Aastrup, T.; Ramström, O. Study of Real-Time Lectin-Carbohydrate Interactions on The Surface of a Quartz Crystal Microbalance. *Biosens. Bioelectron.* **2005**, *21*, 60−66.
(52) Norberg, O.; Deng, L.; Aastrup, T.; Yan, M.; Ramström, O. Photo-Click Immobilization on Quartz Crystal Microbalance Sensors for Selective Carbohydrate-Protein Interaction Analyses. *Anal. Chem.* **2011**, *83*, 1000−1007.
(53) Pei, Y.; Yu, H.; Pei, Z.; Theurer, M.; Ammer, C.; André, S.; Gabius, H. J.; Yan, M.; Ramström, O. Photoderivatized Polymer Thin Films at Quartz Crystal Microbalance Surfaces: Sensors for Carbohydrate−Protein Interactions. *Anal. Chem.* **2007**, *79*, 6897−6902.
(54) Peiris, D.; Markiv, A.; Curley, G. P.; Dwek, M. V. A Novel Approach to Determining The Affinity of Protein-Carbohydrate Interactions Employing Adherent Cancer Cells Grown on A Biosensor Surface. *Biosens. Bioelectron.* **2012**, *35*, 160−166.
(55) Nakahara, S.; Oka, N.; Raz, A. On the Role of Galectin-3 in Cancer Apoptosis. *Apoptosis* **2005**, *10*, 267−275.
(56) Alford, R.; Simpson, H. M.; Duberman, J.; Hill, G. C.; Ogawa, M.; Regino, C.; Kobayashi, H.; Choyke, P. L. Toxicity of Organic Fluorophores Used in Molecular Imaging: Literature Review. *Mol. Imaging* **2009**, *8*, 341−354.
(57) Johnson, A. E. Fluorescence Approaches for Determining Protein Conformations, Interactions and Mechanisms at Membranes. *Traffic* **2005**, *6*, 1078−1092.
(58) Xie, R.; Hong, S.; Feng, L.; Rong, J.; Chen, X. Cell-Selective Metabolic Glycan Labeling Based on Ligand-Targeted Liposomes. *J. Am. Chem. Soc.* **2012**, *134*, 9914−9917.
(59) Iversen, T.-G.; Skotland, T.; Sandvig, K. Endocytosis and Intracellular Transport of Nanoparticles: Present Knowledge and Need for Future Studies. *Nano Today* **2011**, *6*, 176−185.
(60) Sun, S.-S.; Lees, A. J. Synthesis and Photophysical Properties of Dinuclear Organometallic Rhenium (I) Diimine Complexes Linked by Pyridine-Containing Macrocyclic Phenylacetylene Ligands. *Organometallics* **2001**, *20*, 2353−2358.
(61) Ito, H.; Kamachi, T.; Yashima, E. Specific Surface Modification of the Acetylene-Linked Glycolipid Vesicle by Click Chemistry. *Chem. Commun.* **2012**, *48*, 5650−5652.
(62) Pant, C. S.; Wagh, R. M.; Nair, J. K.; Gore, G. M.; Venugopalan, S. Synthesis and Characterization of Two Potential Energetic Azido Esters. *Prop. Explos. Pyrotech.* **2006**, *31*, 477−481.
(63) Percec, V.; Leowanawat, P.; Sun, H. J.; Kulikov, O.; Nusbaum, C. D.; Tran, T. M.; Bertin, A.; Wilson, D. A.; Peterca, M.; Zhang, S.; Kamat, N. P.; Vargo, K.; Moock, D.; Johnston, E. D.; Hammer, D. A.; Pochan, D. J.; Chen, Y.; Chabre, Y. M.; Shiao, T. C.; Bergeron-Brlek, M.; Andre, S.; Roy, R.; Gabius, H. J.; Heiney, P. A. Modular Synthesis of Amphiphilic Janus Glycodendrimers and Their Self-Assembly into Glycodendrimersomes and Other Complex Architectures with Bioactivity to Biomedically Relevant Lectins. *J. Am. Chem. Soc.* **2013**, *135*, 9055−9077.
(64) Polito, L.; Monti, D.; Caneva, E.; Delnevo, E.; Russo, G.; Prosperi, D. One-Step Bioengineering of Magnetic Nanoparticles via a Surface Diazo Transfer/Azide-Alkyne Click Reaction Sequence. *Chem. Commun.* **2008**, 621−623.
(65) Li, X.; Pei, Y.; Zhang, R.; Shuai, Q.; Wang, F.; Aastrup, T.; Pei, Z. A Suspension-Cell Biosensor for Real-Time Determination of Binding Kinetics of Protein-Carbohydrate Interactions on Cancer Cell Surfaces. *Chem. Commun.* **2013**, *49*, 9908−9910.
(66) Ren, Y. J.; Zhang, H.; Huang, H.; Wang, X. M.; Zhou, Z. Y.; Cui, F. Z.; An, Y. H. In Vitro Behavior of Neural Stem Cells in Response to Different Chemical Functional Groups. *Biomaterials* **2009**, *30*, 1036−1044.